Active Optics upgrade using curvature WFS of VISTA for 4MOST

Ronald Holzlöhner, Jérôme Amiaux, Dionisio Garcia-Herreros, Johann Kolb, Jean-François Pirard, et al.

Published version information:

Citation: R Holzlöhner et al. Active optics upgrade using curvature WFS of VISTA for 4MOST. Proc SPIE 12188 (2022): 1218818. Is in proceedings of: Advances in Optical and Mechanical Technologies for Telescopes and Instrumentation V, Montréal, Québec, Canada, 17-23 Jul 2022

DOI: 10.1117/12.2627677

PROCEEDINGS OF SPIE

SPIEDigitalLibrary.org/conference-proceedings-of-spie

Active optics upgrade using curvature WFS of VISTA for 4MOST

Ronald Holzlöhner, Jérôme Amiaux, Dionisio Garcia-Herreros, Johann Kolb, Jean-François Pirard, et al.

Ronald Holzlöhner, Jérôme Amiaux, Dionisio Garcia-Herreros, Johann Kolb, Jean-François Pirard, Stefan Sandrock, William Sutherland , Thomas Szeifert, Gérard Zins, "Active optics upgrade using curvature WFS of VISTA for 4MOST," Proc. SPIE 12188, Advances in Optical and Mechanical Technologies for Telescopes and Instrumentation V, 1218818 (29 August 2022); doi: 10.1117/12.2627677

SPIE.

Event: SPIE Astronomical Telescopes + Instrumentation, 2022, Montréal, Québec, Canada

Active Optics upgrade using curvature WFS of VISTA for 4MOST

Ronald Holzlöhner[1], Jérôme Amiaux[1], Dionisio Garcia-Herreros[1], Johann Kolb[1], Jean-François Pirard[1], Stefan Sandrock[1], William Sutherland[2], Thomas Szeifert[1] and Gérard Zins[1]

[1] European Southern Observatory (ESO), Karl-Schwarzschild-Str. 2, D-85748 Garching, Germany
[2] UK Astronomy Technology Centre (UKATC), Royal Observatory Edinburgh, Blackford Hill, Edinburgh EH9 3HJ, United Kingdom

ABSTRACT

The 4-meter wide-field telescope VISTA will be upgraded with the 4MOST fiber-fed spectrograph. The future field diameter will be 2.5° (before 1.65°) with fast optics of F/3.3, therefore the mechanical alignment tolerances are tight. ESO is currently refurbishing the active optics system based on curvature wavefront sensing, using four technical cameras defocused by ±1.2 mm that image four different stars. We describe the algorithm that computes the telescope misalignment using least-squares fitting, the ESO-developed package *Sensitizer* that generates sensitivity matrices and we discuss maximum likelihood methods.

Keywords: Curvature wavefront sensing, adaptive optics, inverse methods, wide-field telescopes

1 INTRODUCTION

ESO's 4-meter VISTA telescope is located on Cerro Paranal at 2,500 meter altitude. VISTA is a wide-field telescope whose field diameter will be raised from the current 1.65° to 2.5°. The telescope uses fast optics of F/3.3. The existing camera VIRCAM will be replaced by the multi-object fiber-fed spectrograph 4MOST with 2,400 fibers with first science operation in 2004. VISTA has four curvature wavefront sensing cameras around the rim of the focal surface. We image four different stars defocused by ±1.2 mm so that each star appears as the pupil shape, hence the unobscured annular region of the primary mirror. Due to their shape, these images are informally referred to as "donuts". Figure 1 shows VISTA in its closed dome. An overview of the VISTA telescope and the VIRCAM camera has been provided by Sutherland [1].

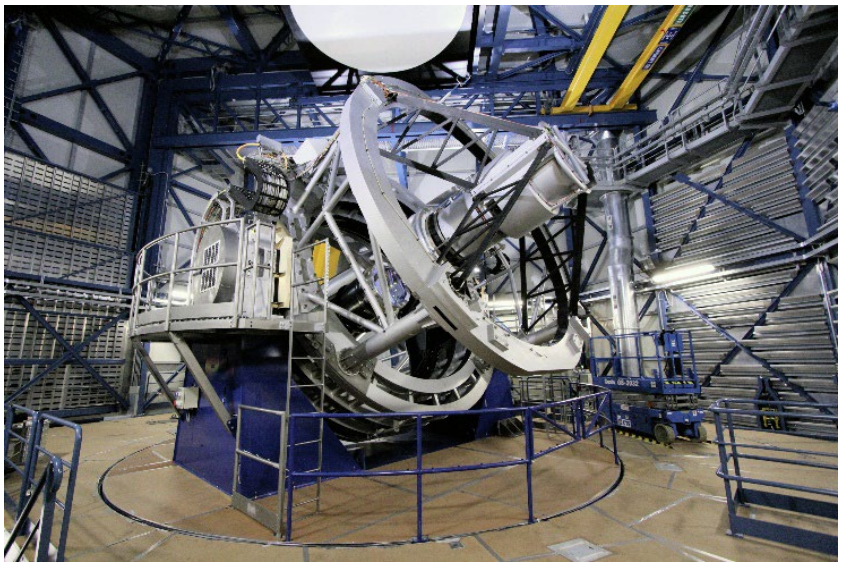

Figure 1: VISTA telescope in its dome

Advances in Optical and Mechanical Technologies for Telescopes and Instrumentation V, edited by Ramón Navarro, Roland Geyl, Proc. of SPIE Vol. 12188, 1218818
 · 0277-786X · doi: 10.1117/12.2627677

In order to maintain good telescope alignment, an active optics system is used that employs four Curvature WaveFront Sensors (CWFS) and corrects the shape of M1 and the position of M2 (primary and secondary mirrors). In the current configuration, two different stars are imaged with a longitudinal focus offset of ±1 mm each. The stars are located on opposite sides of the focal surface science mosaic at a field radius of 0.75° each. Therefore, intra- and extrafocal donuts are recorded for each star so that four donut images are available for processing.

In the future VISTA configuration, there will be six different technical cameras placed on the rim of the science focal plane, as shown in Fig. 2. The cameras are located at azimuth angles of multiples of 60°. Two of the cameras are used for coarse autoguiding (fine guiding is done with an additional fiber-based system) and the other four as CWFS, alternating intra- and extrafocal defocus, with longitudinal offsets of ±1.2 mm. Therefore, four donut images are available again, although each one will record a different star. We use *Spectral Instrument S1900 Cube* cameras with a built-in dewar. The central wavelength of their bandpass filter (645–820 nm) is 732 nm. The bulk of 4MOST, the environment of the technical cameras and the fiber array are not cooled in contrast to VIRCAM, which operated entirely at cryogenic temperatures.

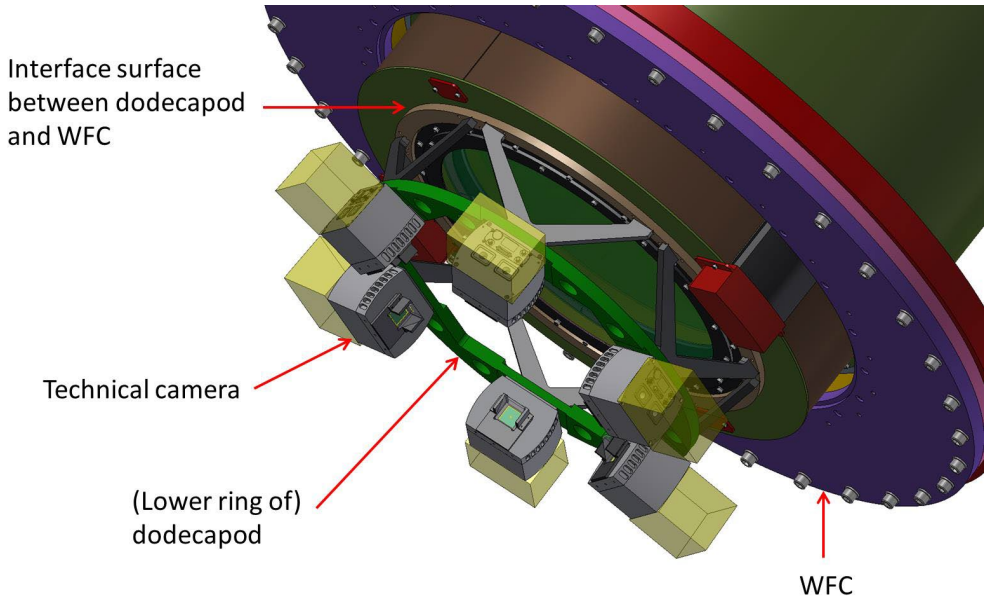

Figure 2: Technical cameras mounted on a dodecapod running around the rim of the science focal plane

In addition to the described so-called low-order wavefront sensors, VISTA-VIRCAM has a dedicated High-Order WaveFront Sensor (HOWFS). It is implemented as a cube beamsplitter mounted in the filter wheel which splits one bright star into two donuts at ±2 mm defocus in J-band (1.2 µm), imaged on a science detector near center field. This HOWFS is run occasionally to calibrate the active optics system and low-order CWFS system and to update look-up tables for telescope alignment correction. In VISTA-4MOST, the HOWFS will be removed. Instead, higher-order optical aberrations can be measured by defocusing the telescope by pistoning the secondary mirror (M2) so as to raise the effective donut defocus to ±2 mm (more precisely, the telescope is defocused in the extrafocal direction and the two corresponding donuts are recorded, then the procedure is repeated with the opposite telescope defocus, recoding the two intrafocal donuts).

The four observed donut images are processed in software so that the misalignment state of the telescope can be reconstructed. The considered misalignment degrees of freedom are five rigid-body degrees of M2 (i.e., not including mirror clocking) and deformations of M1 from the prescribed surface shape, expressed in the Zernike basis. The M2 position is then corrected by sending adjustments to its hexapod and the M1 shape is controlled by 84 pneumatic actuators, arranged in four rings on the backside of M1. These corrections are executed in closed loop throughout the entire night, currently with a default exposure time of 40 seconds and a cycle time of about 55–75 s (this relatively high correction frequency is dictated by observation cadences and may be modified in VISTA-4MOST).

The present processing software has been written by researchers at UKATC, the Rutherford Appleton Laboratory and Durham University which were also part of the consortium that built VISTA-VIRCAM. It is implemented in roughly 30,000 lines of C/C++ code and runs on the telescope workstation and the donut fitting in an LCU (Local Computing Unit). With the switch to 4MOST, a number of technical details in the active optics systems changes: the field radius of the technical stars is raised by the factor 1.24/0.75 = 1.65, we are imaging four different stars whose azimuths, however, are not multiples of 90°, the science field to correct is much larger, and we will allow a degraded mode with only 3 of the 4 donut images available for post-processing. Therefore, the decision was made to rewrite parts of the processing software.

The new software consists of two modules: Firstly the *DonutFitter*, which applies a simplified raytracing method to emulate the donuts under a nonzero WaveFront Error (WFE) and atmospheric turbulence, as seen by the respective WFS. The WFE is expressed in the Zernike basis, and we fit the observed images using the Levenberg-Marquardt (LM) algorithm separately for each donut [8].

The second module is called *TSIM* (Telescope State Inversion Method) which receives the best-fit Zernike modes for each donut and reconstructs the telescope misalignment from the prescribed state, employing maximum likelihood techniques that take the shot noise of each donut image into account. *TSIM* is not specific to CWFS or VISTA and could operate with a variety of wavefront sensing schemes and telescopes.

We will describe *DonutFitter* and *TSIM* in the remainder of this paper.

2 ALGORITHMIC DETAILS

2.1 Curvature wavefront sensing

Curvature WFS take defocused images of a star. Ideally, this image looks like a small copy of the entrance pupil (minus the spider obscurations), usually an annulus. Any wavefront aberrations of the nominal telescope, plus those due to misalignments, will cause brightness variations in the annulus, as shown in the upper row of Fig. 3, which are a function of the wavefront curvature, in turn given by the second lateral derivatives. The theory of curvature wavefront sensing has been first developed and demonstrated by Roddier [2], [3], [4].

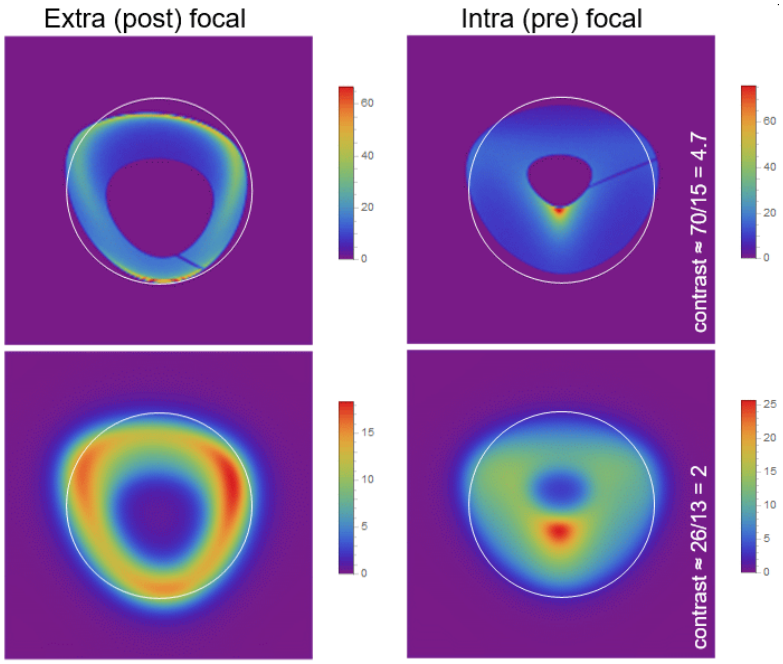

Figure 3: Upper row: Extra- and Intrafocal donut images of the perfectly aligned telescope in the 4MOST configuration, as simulated by *Zemax*. Lower row: Same, after adding a seeing blur of 0.8" seeing. White circles: nominal outer donut rim (Ø = 366 µm = 6.2")

The shape of the donut edges yields the wavefront tip/tilt near the inner and outer pupil rims, given by the *first* derivatives of the WFE. Starting from the donut edges and progressing inside the donut annulus, the WFE can then in principle be derived through double integration. The distortion of the donut shape, and hence the implied irregular coordinate transform from a ray interception with the entrance pupil to its landing point on the detector, complicates CWFS significantly.

Moreover, the donut image is distorted by atmospheric turbulence (which varies with the field point, depending on the height of the turbulent layers), detector noise and possibly other imaging artifacts, including (non-common) path aberrations due to different beam footprints and WFS optics. In contrast to the Shack-Hartmann WFS that only extracts beam centroids and no higher-order spot shape variations, atmospheric blur and parasitic aberrations are convolved with the desired sensor signal in a more complicated way. These disadvantages must we weighed against the simple detector architecture of CWFS, working with fixed detectors without the need for pickoff arms with an actuator mechanism.

Roddier's method consists of approximating the solution of the Irradiance Transport Equation (ITE or TIE), which links the longitudinal irradiance evolution $\partial I/\partial z$ to the wavefront curvature. The term $\partial I/\partial z$ is approximated by the discrete difference S between extra- and intrafocal donut images of the same star, divided by the double donut defocus. The wavefront curvature, in turn, is approximated by integrating S twice using the discrete Fourier transform. After masking and conditioning of the wavefront on the rim, one computes a new estimate of S by evaluating the Laplacian of the wavefront. One then iterates until convergence is achieved between the WFE and S. A good discussion of implementing this iteration is given by Xin *et al.* [5].

However, Roddier's scheme has a number of disadvantages: a) the discrete difference approximation of $\partial I/\partial z$ is only accurate to first order, b) the first wavefront derivative at the donut rim, which also appears in the ITE, requires special treatment, c) one needs a beam splitter to generate two images of the same star, each receiving only half of the photons, implying some information redundancy. An additional serious limitation comes from the implicit assumption that there is a one-to-one mapping between points in the extra- and intrafocal pupils. In other words, it is assumed that the rays do not cross each other except directly at the focus, so that there is no caustic in any donut. In the latter situation, a point in one of the donut images may be struck by rays from two different, even disconnected, areas in the other donut. This situation will lead to a local error in Roddier's algorithm and the only way to prevent it is to raise the defocus. However, then the donut images overlap with a larger area on sky and look more regular, thus decreasing the irradiance variation with WFE and hence the sensitivity. Optimizing the sensor defocus thus involves a trade-off between the signal-to-noise ratio (SNR) for dim technical stars (i.e., high sky coverage in bright nights) and the risk of overlapping donuts in crowded star fields, both of which favor smaller donuts, versus accommodating the worst combination of telescope misalignment and seeing that the CWFS is required to work in without completely distorting the annulus shape of the donuts. We chose ±1.2 mm in VISTA-4MOST.

There are other ways of solving the ITE such as direct Zernike mode decomposition of the differential equation. Xin has implemented that method and tried it at the Simonyi Survey Telescope (previously called LSST), but reports it suffering from other limitations.

Instead of "splitting stars", it is also possible to work with a single donut image of each star, as discussed by Wu *et al.* [6]. Wu reconstructs the WFE by first binning the detector image into small patches and then approximating the derivatives $\partial I/\partial Z_k$ for each patch by discrete differences, where the Z_k are the coefficients of the WFE expanded in the (annular) Zernike polynomial basis. Then a linear equation is obtained that approximates the ITE piecewise and is finally solved for the Z_k by matrix inversion. The advantage of single donut images is that each detector can image a different star, thus one can use more stars and cover the science focal plane more efficiently, thus improving the conditioning of the telescope misalignment degrees of freedom as a function of the observed noisy WFE.

In this work, we adopt the single star image approach with four technical stars enclosing the science field, but employ simplified paraxial raytracing combined with least-squares iteration to fit the Zernike coefficients, using the local derivatives $\partial I/\partial Z_k$ to accelerate convergence. We therefore do not suffer from first-order accuracy limitations, the fit uses no linearization and we can deal with strong WFE, including caustic ray crossing and highly distorted donuts.

2.2 Donut Fitter

If the telescope is well aligned, the donuts look almost like circular annuli, as shown in Fig. 4. However, due to the significant spherical aberration, the central hole has very different relative sizes between extra- and intrafocal donut images. The slight left-right asymmetry in the images is due to the off-center location of the donut on the detector. The simulation was carried out with *Zemax OpticStudio* using the *Geometrical Image Analysis* tool which simulates a detector with

selectable resolution, hit by a few million rays. A blur has been added to the lower row donuts in post-processing by convolution with a Moffat function kernel ($\beta = 2.1$), corresponding in width to a seeing of 0.8" at 500 nm. It is evident that the blur lowers the image contrast and thus costs SNR, in particular on the higher-order modes. A single spider has been simulated for illustration (the spiders are 36 mm wide), but the shadow is all but washed out by the seeing. All post-processing in these tests, including the atmospheric blur, is done in *Mathematica* using custom code written by the authors.

We employ a simplified raytracing scheme in which we start with the donut shapes of the nominal telescope. The actual ray landing positions q_j in the donut due to nonzero WFE in a misaligned telescope are then controlled by the WFE Zernike coefficients Z_k. More precisely, the lateral position offsets from the nominal ray landing positions q_j^{nom} are proportional to the Zernike slopes in the focal plane, which we pre-calculate analytically in *Mathematica* and then evaluate at a grid of about 1300 sample ray crossing positions p_j with the entrance pupil, taking into account the obscurations due to the four spider veins and M2. We express $q_j = q_{\mathrm{Re},j} + i\, q_{\mathrm{Im},j}$ and the *x*/*y* slopes of the Zernike functions z_k for convenience in the complex plane by $D_{jk} = \partial z_k(p_j)/\partial x + i\, \partial z_k(p_j)/\partial y$, where i is the imaginary unit, and write

$$q_j = q_j^{nom} - \sum_k D_{jk}\, Z_k. \qquad (1)$$

This way, we exploit *Mathematica's* strong analytical capabilities for extremely fast raytracing. Next, we quantize the q_j on a virtual detector that corresponds to the detector emulated in *Zemax* and count the number of received rays in each pixel. Typically, we oversample the image by the factor 2 compared to the technical CCD detector chips e2v-42 which has a pixel size of 13.5 µm (0.227" on sky). Finally, we convolve the raytraced image with the seeing blur as described above, where the seeing value (more precisely the image quality at the observing wavelength) becomes an additional fit variable.

The observed donut image first undergoes some image processing in which we locate the donut in a window region read from the detector and apply a mask to reject background stars, sky background and detector noise further away from the donut. The synthetic, raytraced image data is scaled to have the same total number of detector hits (detected photoelectrons) as the observed donut and both donuts are shifted so that their barycenters lie at their respective image centers. However, no rotation or size scaling is performed. The objective function f to be minimized equals the squared differences in the image brightness between the raytraced, synthetically generated donut (Fig. 4 left column, I_{syn}) and the observed donut

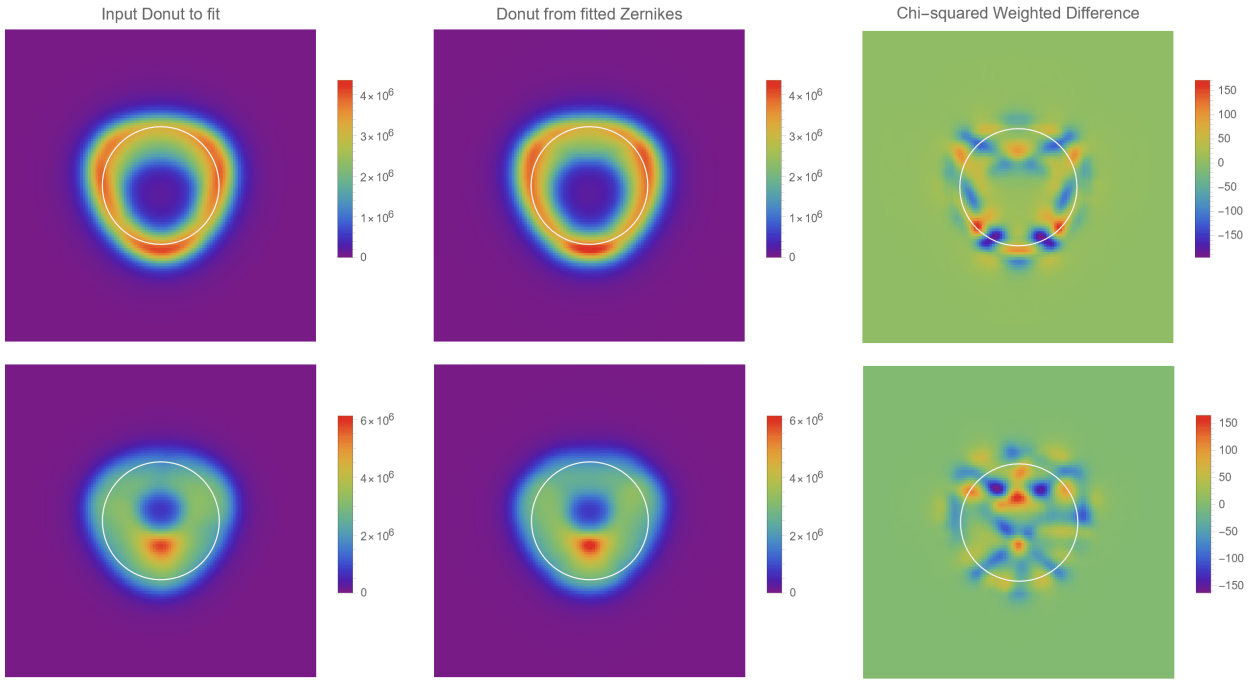

Figure 4: Left column: Extra- (top) and Intrafocal (bottom) donut images of two detectors in the perfectly aligned telescope, as simulated by *Zemax*, with added seeing blur of 0.8", center column: numerically approximated donut from our simplified raytracing, right column: chi-squared weighted image difference used as objective function in the fit.

(Fig. 4 center column, I_{obs}), divided by I_{obs}. The sum runs over all illuminated detector pixels j

$$f = \frac{1}{2}\sum_j r_j{}^2 \quad , \qquad r_j = \frac{I_{syn,j} - I_{obs,j}}{\sqrt{I_{obs,j}}} \quad . \tag{2}$$

The denominator in Eq. (2) thus equals the variance of the Poisson-distributed shot noise and implements importance weighting; a maximum likelihood technique (the variance of a Poisson-distributed stochastic quantity equals its mean). The function f is also known as a chi-squared metric (Fig. 4 right column) [8]. Effectively, the dimmer portions of the donut, notably its inner and outer rims, become somewhat emphasized.

The number n of Zernikes to be fitted can become rather high such as $n = 25$ or even $n = 34$ when fitting higher-order WFE. In VISTA-VIRCAM, the Nelder-Mead minimization algorithm was used which forms an n+1-dimensional simplex that converges to a local, and hopefully the global, function minimum. This method is robust but slow, limiting us to $n = 5$. In the new implementation, we employ the Levenberg-Marquardt (LM) algorithm instead, which is an adaptive mix of steepest descent (proceed in the direction of the strongest function decrease, determined by the local Jacobian $\partial I/\partial Z_k$) and the Newton methods (quadratic function approximation near the minimum). We find that the LM method applied to *Zemax* generated test images often converges within 4–6 steps, completing in under 2 seconds on a modern workstation. Moreover, the four donuts can be processed in parallel.

Figure 4 shows a comparison of simulated donuts in *Zemax* (left column) with the best fit (center column). The right column shows the images of the r_j in Eq. (2).

The optical model contains two more notable complications: Firstly, the CCDs with 2048×2048 pixels and a linear size of 27.7×27.7 mm^2 have a significant extent compared to the focal surface radius of 268 mm. We have therefore computed the Zernikes of the nominal telescope on a grid of 5×5 samples on the detector and use spline interpolation to derive accurate Zernikes at the location of the donut center. Secondly, VISTA-4MOST includes an Atmospheric Dispersion Compensator (ADC) consisting of two counter-rotatable wedge pairs, each consisting of two different glasses with different refractive indices. We compensate for the Zernike aberrations of the ADC as a function of ADC rotation angle.

2.3 Donut fit results

Any misalignment manifests as a donut deformation/contortion that depends in a complicated manner on the camera

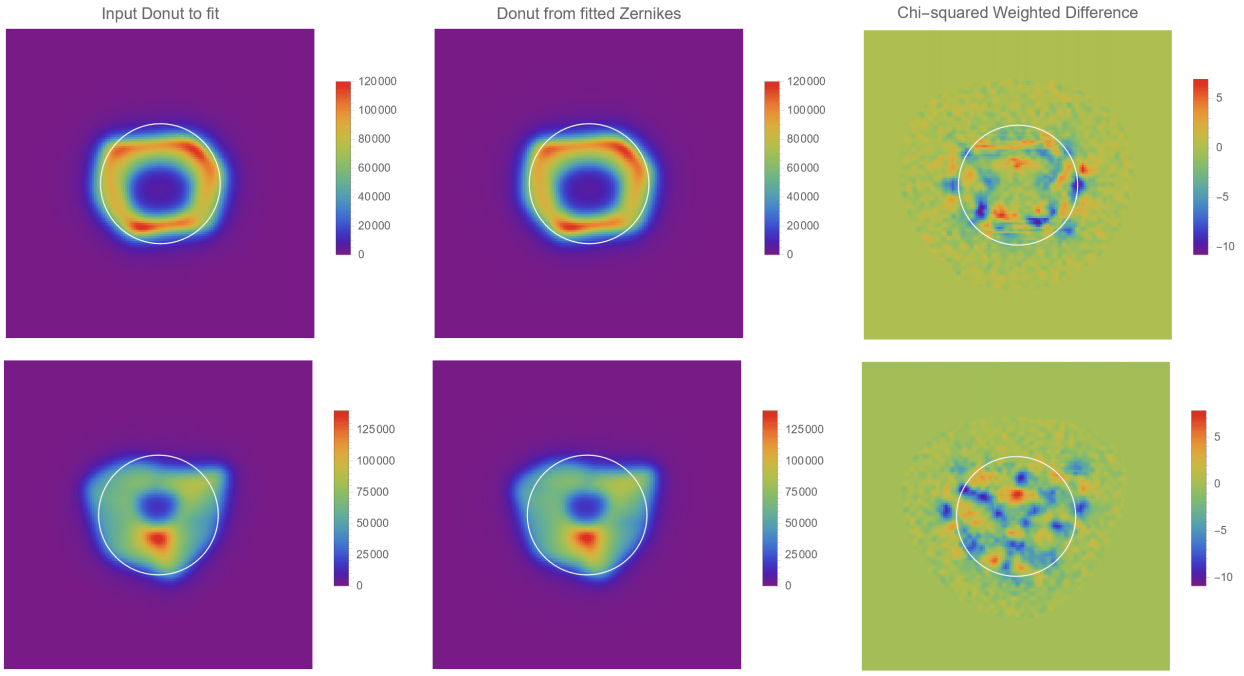

Figure 5: Left column: Extra- and intrafocal donut images of the *misaligned* telescope, as simulated by *Zemax*, with added seeing blur of 0.8", center column: numerically approximated donut from simplified raytracing, right column: chi-squared weighted difference

location and the type of misalignment, as shown in Fig. 5. The misalignment is a combination of M2 decenter (x: 30 µm, y: −22 µm, piston: 4 µm), tip (35 µrad), tilt (23 µrad) and some measured M2 figure aberrations, which are to first order compensated on M1. Since the beam footprint wander across M1 depending on the field point, this compensation can only work for a single field point at the most. Unfortunately, the measured VISTA M2 figure aberrations are very large and depend on telescope altitude, causing an OPD of about 1000 nm RMS astigmatism and 700 nm trefoil, to name only the leading two terms. They are likely caused by the strongly lightweighted M2 whose face sheet has a thickness of only 25 mm and shows a print-through of its 3-point mount and the 12-count rib structure.

We have runs a large set of test cases and are not aware of a single case in which the algorithm converged to a local minimum corresponding to an image obviously different from the simulation result. The number of iterations until convergence is actually lowered by the turbulence blur, presumably because the objective function becomes smoother.

Table 1 shows a comparison of the best fit Zernike coefficients with the coefficients computed by *Zemax* for the misaligned telescope at the donut center for one star. The total RMS fit error is 23.7 nm. The detector image was emulated with added shot noise and a seeing of 0.8" (defined at 500 nm) in the limit of maximum brightness just before saturating the detector. The fit looks very good and the fit error is probably close to the smallest achievable one.

Table 1: Best fit Zernike coefficients Z_k of the extrafocal donut shown in the upper row of Fig. 5. Third column: Zernike coefficients on the detector obtained from *Zemax*, last column: fit error. All numerical values are in nanometer RMS.

Z#	Best Fit ΔZ [nm RMS]	Commanded ΔZ [nm RMS]	Fit–Commanded [nm RMS]
z4	−217.	−208.4	−8.6
z5	35.3	42.9	−7.6
z6	432.6	440.	−7.4
z7	23.1	22.7	0.3
z8	16.9	12.	5.
z9	106.9	119.7	−12.8
z10	−28.3	−31.5	3.2
z11	6.4	4.9	1.5
z12	68.9	64.9	4.
z13	−15.1	−17.2	2.1
z14	−137.3	−130.1	−7.3
z15	−55.2	−54.5	−0.6
z16	−1.	−0.5	−0.6
z17	5.3	−1.	6.2
z18	2.	0.9	1.1
z19	10.	7.4	2.6
z20	−5.	0.5	−5.5
z21	−1.	−0.5	−0.5
z22	0.6	−0.2	0.8
z23	−1.8	0.1	−1.9
z24	−3.2	−0.5	−2.8
z25	−0.7	−1.2	0.5
z26	5.1	2.3	2.8
z27	54.2	54.3	0.
z28	25.1	25.3	−0.2

Table 2 shows the fit statistics summary for all four donuts. We define the normalized ζ' error metric based on work by Gavin [8] as

$$\zeta' = \sqrt{\frac{2\,f}{v\,(n_b - n + 1)}}\,, \qquad v = \frac{\sqrt{p^2 + {g_1}^2}}{g_2}, \tag{3}$$

where f is the final value of the objective function, n_b is the number of bright (subsampled) pixels, p is the total number of detected photons in the donut and $g_1 = 1.37\times10^7$; $g_2 = 5.14\times10^7$ are constants. This metric implements a fitting error per illuminated pixel and divides it by the term v, which approximately equals the shot noise variance. The purpose is to compare the value of ζ' to an absolute error threshold so that we can decide on the goodness of fit for a wide range of star brightnesses and exposure times. If the metric exceeds a certain value, our application automatically reruns the fit with starting values of ±1250 nm RMS initial defocus. The other initial values of the Zernike coefficients are near zero.

The SNR is defined as $p/(n_b\, b)$, were b is the sky background per pixel. We compute b as the median value of the outer rim of the received image and subtract it from the image data. However, the background is of course afflicted by shot noise, hence it always deteriorates the image. In our emulated donuts, we used a (dim) sky background of magnitude 17.9.

The Pearson correlation equals the convolution of the observed image after background subtraction with the nominal (simulated) donut image at the same resolution), normalized by total irradiance. The peak of the 2D convolution result is then taken as the image center and the contiguous area around it (which is in general not exactly circular) defines a mask to identify and crop out the relevant donut region, rejecting unwanted background.

One can see that a small number of iterations of 3–6 can be sufficient for the LM algorithm to converge to a solution in the presence of a seeing of 0.8". However, we remind the reader that the donuts were emulated with *Zemax* and while we did add shot noise to the image, the star brightness was very high and actually close to the detector (full well) limit. We have also tested various cases with inferior SNR and sets of stars with strongly differing brightness.

Table 2: Donut fit summary. Columns: CWFS number, residual ζ-metric of fit, RMS Zernike error to *Zemax* solution, best fit seeing, wall clock run time for each fit, iteration number of LM algorithm, fit status (0 = success), Pearson correlation of observed donut with nominal donut and average SNR per (oversampled) pixel.

CWFS #	χ residual [e−]	ΔZ fit error [nm]	seeing ["]	time [s]	steps	status	Pearson correlation	SNR per sample
1.	2.17	23.66	0.8	3.9	6.	0.	0.93	25.22
2.	2.49	32.17	0.8	2.85	4.	0.	0.98	25.17
3.	2.15	31.97	0.8	3.2	4.	0.	0.95	25.19
4.	2.36	23.78	0.8	2.5	3.	0.	0.98	25.18

We also continuously compute the Jacobians J of each (sub)pixel value I_j in a given donut image with the elements J_{jk} from which we compute the variance-covariance matrix V of the Zernike coefficients [8] as

$$J_{jk} = \frac{\partial I_j}{Z_k}\ , \quad J_{st} = [J_1, J_2, J_3, J_4]\ , \quad V = \left[{J_{st}}^T \cdot J_{st} \right]^{-1}, \tag{4}$$

where J_{st} is "stacked" by combining the four Jacobians through joining columns. The superscript −1 denotes the matrix inverse. In Fig. 6, the left plot shows the square root of the principal diagonal of V, hence the uncertainty of the fitted Zernike modes caused by shot noise. The higher-order Zernike modes are less influenced by the shot noise because their slopes are higher (the Zernike functions are steeper) than those of the low-order modes. Therefore, the error propagation is weaker. In fact, we can see that shot noise does not matter in the presented limit of very bright stars.

The right plot in Fig. 6 shows the total fitting error as compared to the Zernike modes derived by *Zemax*. The errors in the modes Z5/Z6 (astigmatism) and Z14 (tetrafoil 0°) are higher than in the other modes; possibly caused by image elongation as discussed in the next paragraph.

The VISTA-4MOST exit pupil distance from the detector (4312 mm) does not agree with the focal surface radius (4653 mm). Because the flat CCD detectors of 39.1 mm diagonal are oriented tangentially to the focal surface, the chief ray does not impinge on the detectors exactly orthogonally to the surface, causing a small image elongation along the tilt direction. Another example of systematics is the geometrical error term that arises when considering a WFE defined on top of a strongly curved wavefront, as is the case in a wide-field telescope at $F/\# = 3.3$, when using a detector that is not curved in the same way, but flat. As a consequence, the lateral ray offset as a function of the WFE slope grows with the pupil radius. However, the relative deviation amounts to below 1% in VISTA-4MOST. Moreover, no diffraction effects are accounted for in our raytracing, or in the *Zemax* model. Diffraction will therefore be an additional error when working

with observed donuts. We can conclude that there are (systematic) error sources other than shot noise in the simplified raytracing model that may even dominate the total error in some cases.

For simplicity, we choose to work in the basis of standard Zernike polynomials. This basis is convenient because the functions are well known and not difficult to differentiate. However, there are a number of caveats: a) The standard Zernikes are defined on the entire unit disk while the pupil of a (wide-field) telescope is only an (near) annulus, furthermore with a central obscuration decentered by an amount depending on the field point; b) Even if the pupil did equal the full

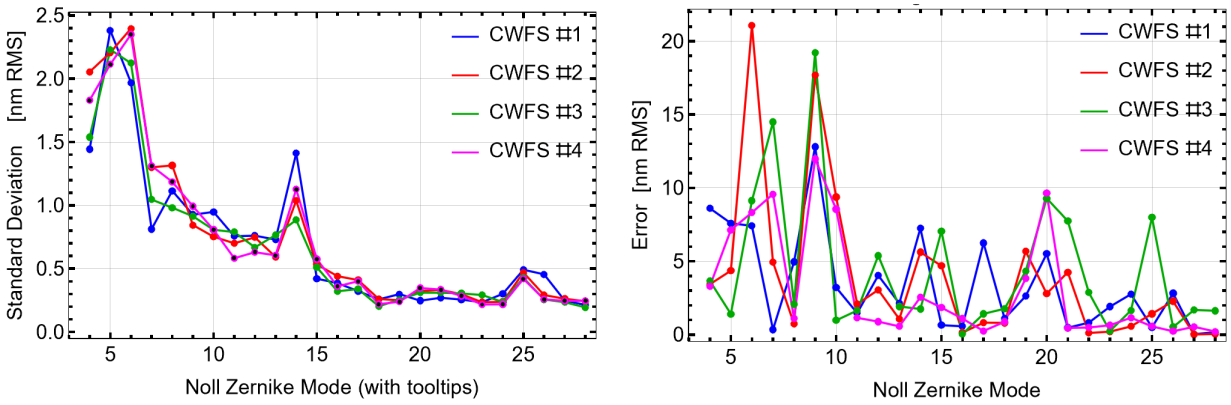

Figure 6: Left: Zernike coefficient uncertainty due to shot noise. Right: Zernike fit error, compared to *Zemax*

unit disk and assuming there is no caustic ray cross-over, the Zernikes would still not be orthogonal when considering the donut images, whose local brightness depends on the second WFE derivatives; c) the shape of M1 is controlled by actuators that bend the mirror shell. Since the mirror is very stiff, it is more useful to consider the mirror bending eigenmodes, which only roughly correspond to some Zernikes. Finally, we have to remember that the beam footprint varies with the field point and is defined by the stop surface, which is M2. The beam footprint on M1 wanders laterally by up to 200 mm.

As a consequence of the discussion in the previous paragraph, it is plausible that the fitted Zernike coefficients vary somewhat when the number of Zernike modes to be fitted is changed by the user. We found this effect in our runs, although it does not seem to influence the telescope reconstruction results very much.

Since the active optics system of VISTA-4MOST is under construction, we are limited to *Zemax*-generated test donuts to validate the new optical configuration. On the other hand, we have also run *DonutFitter* on observed donuts obtained with VISTA-VIRCAM. We find in our initial simulations that a larger number (several tens) of iterations is needed. Moreover, the best fit Zernike coefficients of the extra- and intrafocal donuts pertaining to the same star differ by significant amounts. Despite these points, we can however still reconstruct the telescope misalignment state. Our studies on the subject are ongoing.

2.4 Telescope misalignment state reconstruction

In the second step, we have to map the fitted Zernike coefficients Z to telescope misalignment parameters p such as the rigid-body degrees of freedom of M2 and the surface deformation modes of M1. We consider the Generalized Least-Squares problem [9] (not to be confused with the least-squares problem arising in the donut fitting)

$$\min \rho^T V^{-1} \rho \quad , \qquad \rho = Sp - Z, \tag{5}$$

where S is the optomechanical sensitivity matrix converting misalignments to WFE and ρ denotes the reconstruction residual. The objective is to make the 2-norm of ρ as small as possible, weighted by the inverse of the variance-covariance matrix V defined in Eq. (4).

The unbiased estimator for p is given by the following linear equation [9]

$$\rho = TZ \quad , \qquad T = (S^T V^{-1} S)^{-1} S^T V^{-1}. \tag{6}$$

The sensitivity matrices are computed by the ESO software package *Sensitizer* [7], which drives *Zemax OpticStudio* through a .NET API. *Sensitizer* disturbs the telescope prescription in each degree of freedom in turn by very small amounts while recording the variations in the WFE, expanded in Zernike coefficients.

The sensitivity matrix is precomputed, its elements are interpolated by the first three Fourier terms and, during telescope operation, evaluated numerically at each donut position. Finally, the four matrices are stacked up to be joined into a single matrix, inverted and multiplied by the stacked vector of the best fit Zernikes (e.g., when fitting the 25 Zernike modes from Z4 (defocus) to Z28 (hexafoil), of length 4×25 = 100), as shown by Eq. (6).

An important aspect is to keep the condition number cond(S) of S, defined as the ratio between the largest and the smallest singular value, as small as possible in order to limit the error propagation. This number depends on the selection of perturbations to include into S. We manage to limit cond(S) to about 150 by selecting appropriate Zernike Sag modes on M1 and M2. We include Z5, Z6 plus Z9–Z28 on M1 and Z9–Z28 on M2 in the inversion. We thus exclude the coma modes (Z7, Z8) on M1 which lead to ambiguities versus the M2 position and would raise cond(S).

We call this method of first fitting the donut individually in the Zernike basis and then computing the ρ of the maximum likelihood by matrix inversion a *backward*, or inversion, telescope reconstruction method. One may object that the fitting space dimension of 4×(25+1) = 104 fit variables is much larger than the dimension of the telescope misalignments, which may only have on the order of 10–20 dimensions. As a consequence, most combinations of Zernike modes do not correspond to a physically possible misalignment state of the telescope. Since the CPU effort of fitting grows with the number of variables, one may argue that this situation is inefficient.

Indeed, in VISTA-VIRCAM, two stars were split into extra- and intrafocal images whose Zernike modes must each agree. Therefore, only two runs of the fit routine were done, each of which fit the extra- and intrafocal images of one star at the same time. In cases of high noise and/or poor seeing, this approach may keep the fitter "on track" and prevent running into some impossible solutions in Zernike space. Since the two WFS were located on opposite sides of the optical axis, it was moreover easy to exploit the symmetry and derive the solution p using very simple equations rather than explicit matrix inversion.

Even in VISTA-4MOST that images four different stars, a similar scheme would be possible as follows: The fitter actually runs in the space of the telescope misalignments p, from which $Z = Sp$ is computed for all four donuts and then all donuts are fitted in the same iteration, deriving a combined chi-squared error metric. We also implemented this *forward* reconstruction method, but found that it has a few disadvantages: It often required a large number of fitting steps, presumably because the topology of the space of the function $f(p)$ is more complicated than the space of $f(Z)$ of a single donut (for instance, the fitting routine may have trouble in situations where the fit improves for one donut and worsens for another). Feeding the Jacobian $\partial r_j/\partial p_k$ into the LM algorithm may help. Secondly, it is not as easy to parallelize the fitting to be done on the individual donuts (the parallel threads are more fine grained). The topic deserves further investigation.

Imaging four donuts located around the focal surface provides us with the luxury of some redundancy and we can actually solve the inversion problem with only three donuts. The latter is very beneficial in case one of the images is garbled for some reason, polluted by a bright background object, or simply too dim. We have implemented a heuristic to detect such cases and automatically ignore deficient donuts.

3 RESULTS & DISCUSSION

3.1 Investigations

The telescope state reconstruction yielded the results described in this section. The total residual WFE after applying the computed corrections $Sp - Z_{zx}$, where Z_{zx} denotes the WFE computed by *Zemax*, is 27 nm RMS. We thus see that the inversion process has not added much error to the donut Zernike fit. Table 3 shows the RBM modes for M2, as computed by *TSIM*.

Table 3: Rigid-Body Modes (RBM) of M2. Reconstructed: Values found by *TSIM*, Commanded: Misalignments entered in the *Zemax* simulation, Uncertainty: Standard deviation in the Zernike Sag modes from error propagation

RBM mode	Reconstructed	Commanded	Recon–Cmd	Uncertainty
dx [μm]	30.9	30.	0.9	2.2
dy [μm]	−21.3	−22.	0.7	2.3
dz [μm]	4.	4.	0	0.1
dRx [μrad]	34.7	34.9	−0.2	1.2
dRy [μrad]	22.4	22.7	−0.3	1.2

Table 4 shows the Zernike Sag modes for M2. The meaning of the columns is similar to the columns in Table 3. The additional column “Cmd residual” denotes *Zemax* values after balancing M1 versus M2 figure aberrations (TSIM cannot decide for some low-order modes if a surface error originates on M1 or M2, but the difference may not be crucial, so we map all such errors onto M2, which is where *Zemax* simulated it).

Table 4: M2 figure deformation (“Zernike Sag modes”).

Zernike Noll mode	Reconstructed [nm]	Commanded [nm]	Recon–Cmd [nm]	Uncertainty [nm]
9.	−329.3	−364.6	35.3	6.7
10.	−1.2	−4.6	3.4	6.4
11.	−2.5	0	−2.5	3.5
12.	36.4	36.3	0.1	3.4
13.	−9.4	−10.4	1.	3.5
14.	−4.6	−5.3	0.7	4.6
15.	−86.8	−89.4	2.6	4.3
16.	−1.	0	−1.	2.4
17.	−0.1	0	−0.1	2.3
18.	−15.8	−15.6	−0.3	2.4
19.	−83.1	−78.	−5.1	2.5
20.	−67.	−68.5	1.5	3.
21.	49.3	47.4	2.	3.4
22.	1.3	0	1.3	2.
23.	−0.1	0	−0.1	2.
24.	−0.8	0	−0.8	2.
25.	−1.4	0	−1.4	2.1
26.	0.4	0	0.4	2.
27.	22.8	28.6	−5.8	2.5
28.	10.2	13.4	−3.1	2.5

Table 5: M1 figure deformation (“Zernike Sag modes”).

Zernike Noll mode	Reconstructed [nm]	Commanded [nm]	Cmd Residual [nm]	Recon–Cmd [nm]	Uncertainty [nm]
Z5	0.9	−45.8	0	0.8	2.8
Z6	7.4	−655.1	0	7.4	2.8
Z9	−429.4	−461.8	−461.8	32.4	7.7
Z10	−4.3	−5.8	−5.8	1.6	7.5
Z11	−2.2	0	0	−2.2	3.9
Z12	56.5	50.2	50.2	6.3	3.9
Z13	−12.1	−14.3	−14.3	2.2	3.9
Z14	−9.2	−7.2	−7.2	−2.	5.6
Z15	−119.1	−123.2	−123.2	4.1	5.3
Z16	−1.4	0	0	−1.4	3.
Z17	1.	0	0	1.	3.
Z18	−22.9	−23.4	−23.4	0.5	3.
Z19	−121.	−116.8	−116.8	−4.2	3.2
Z20	−98.4	−102.8	−102.8	4.3	4.
Z21	71.6	71.1	71.1	0.5	4.7
Z22	1.3	0	0	1.3	2.5
Z23	0	0	0	0	2.6
Z24	−1.	0	0	−1.	2.4
Z25	−0.1	0	0	−0.1	2.6
Z26	−0.2	0	0	−0.2	2.6
Z27	−9.	0	0	−9.	3.5
Z28	−4.7	0	0	−4.7	3.6

4 CONCLUSIONS

We are upgrading some parts of the active optics (ActO) system of VISTA when removing the VIRCAM camera and replacing it by 4MOST, a fiber-fed spectrograph. At the same time, the science field diameter is raised from 1.65° to 2.5°, making the accuracy of the telescope alignment more critical and challenging. The new ActO system uses Curvature WaveFront Sensors (CWFS) imaging four different stars around the science field and employ a new post-processing algorithm to reconstruct the telescope misalignment state. In the first step (*DonutFitter*), the wavefront error *Z* expanded in the Zernike basis is fit to each defocused star image, informally known as "donuts". We simulate the image formation using fast simplified raytracing. In the second step (*TSIM*), we reconstruct the telescope misalignment state by inverting the optomechanical sensitivity matrix (the derivatives of the wavefront error by all mechanical misalignments) and multiplying by *Z*. We add that *TSIM* uses maximum likelihood techniques, is independent of CWFS and is indeed applicable to a wide range of optical systems.

We have developed and implemented the algorithm in *Wolfram Mathematica*. The development process is rapid, thanks to the strong graphical and analytical abilities. We also benefitted from previous work at ESO such as *Sensitizer*, which computes the sensitivity matrices. We chose a step-by-step approach in which we first tested the optics basics like the simplified raytracing and then grew the complexity by combining subroutines. Certain low-level time-critical operations like counting rays on a virtual detector were automatically converted to the C language and compiled. The executive decision was taken later to implement the production code in *Matlab* and therefore, *DonutFitter* and *TSIM* have been translated for deployment on the VISTA workstation.

We have tested the algorithm on a wide range of test cases simulated in *Zemax* and find that it is robust and has low error down to a limiting magnitude of about 17 in the faintest star. The algorithm has further been adapted to work with calibration donuts recorded in the ActO system of VISTA-VIRCAM and we are in the process of reducing these data. The new algorithm will be tested on VISTA starting in November 2022.

REFERENCES

[1] W. Sutherland, J. Emerson, G. Dalton *et al.* "The Visible and Infrared Survey Telescope for Astronomy (VISTA): Design, technical overview, and performance", Astron. & Astrophys 575, A25 (2015)

[2] C. Roddier and F. Roddier, "Wave-front reconstruction from defocused images and the testing of ground-based optical telescopes," J. Opt. Soc. Am. A 10, 2277–2287 (1993).

[3] F. Roddier, "Curvature sensing and compensation: a new concept in adaptive optics," Appl. Opt. 27, 1223–1225 (1988)

[4] F. Roddier and C. Roddier, "Wavefront reconstruction using iterative Fourier transforms," Appl. Opt. 30, 1325–1327 (1991)

[5] B. Xin, C. Cleaver, M. Lliang *et al.,* "Curvature wavefront sensing for the large synoptic survey telescope", Appl. Opt. 54 (2015)

[6] Wu Z., Bai H. and Cui X., "Curvature wavefront sensing based on a single defocused image and intensity compensation," Appl. Opt. 55, 2791–2799 (2016)

[7] R. Holzlöhner, A. Kellerer, U. Lampater, S. Lewis, C. Zanoni, "Structural, thermal, and optical performance analysis applied to subsystems of the European Extremely Large Telescope", J. of Astron. Telescopes, Instruments and Systems 8, 021504 (2022)

[8] H. P. Gavin, "The Levenberg-Marquardt algorithm for nonlinear least squares curve-fitting problems", script Duke University (2020); online [https://people.duke.edu/~hpgavin/ce281/lm.pdf]

[9] M. R. Osborne "Least squares and maximum likelihood", online at [https://maths-people.anu.edu.au/~mike/lsnml.pdf]